

Speckle Tracking in 3D Echocardiography with Motion Coherence

Xubo Song¹, Andriy Myronenko¹ and David J. Sahn²
Dept. of Computer Science and Electrical Engineering¹
OGI School of Science and Engineering¹
Cardiac Fluid Dynamics and Imaging Laboratory²
Oregon Health and Science University^{1,2}

xubosong@csee.ogi.edu, myron@csee.ogi.edu, sahnd@ohsu.edu

Abstract

Tracking of speckles in echocardiography enables the study of myocardium deformation, and thus can provide insights about heart structure and function. Most of the current methods are based on 2D speckle tracking, which suffers from errors due to through-plane decorrelation. Speckle tracking in 3D overcomes such limitation. However, 3D speckle tracking is a challenging problem due to relatively low spatial and temporal resolution of 3D echocardiography. To ensure accurate and robust tracking, high level spatial and temporal constraints need to be incorporated. In this paper, we introduce a novel method for speckle tracking in 3D echocardiography. Instead of tracking each speckle independently, we enforce a motion coherence constraint, in conjunction with a dynamic model for the speckles. This method is validated on in vivo porcine hearts, and is proved to be accurate and robust.

1. Introduction

The aging population in the much of the world has survived the risk of coronary disease as a cause of death and now faces future health risks for ischemic or non-ischemic cardiomyopathy and heart failure. Aggressive approaches to pharmacological, surgical, and resynchronization therapies for heart failure treatment require an improved understanding of myocardial motion the fundamental mechanics which determine Left Ventricular function. Cardiac motion is a combination of apex-to-base lengthening or shortening with simultaneous twisting, and study of heart function needs to be able to capture such complex 3D deformations which occur during left ventricular contraction and relaxation.

The vast majority of research on quantitative analysis of heart deformation has been based on tagged MRI [10], which provides superior image resolution and soft tissue

characterization. However, it is difficult to apply MR for acute myocardium infarction or patients with pacemakers, and tracking tags over the complete cardiac cycle is difficult due to tag decay over time. Echocardiography provides an attractive alternative for its portability, bedside applicability, low cost, and safety. It has long been a popular modality for cardiac imaging. Recently there has been increasing interest in using echocardiography, specifically using speckle tracking, as a tool to analysis heart deformation.

Speckles are formed by the interference of the backscattered echoes produced by ultrasonic scatterers in tissue and blood. The speckle at a given location is characterized by a unique texture pattern. The speckles follow the motion of the myocardium so when the myocardium moves from one frame to the next, the position of this pattern will move accordingly. The assumption for speckle tracking is that when the myocardium undergo mild deformation and when the temporal sampling rate is adequately high, the speckles remaining fairly constant, and thus makes tracking possible.

Most of the current speckle tracking methods are based on 2D echocardiography, where the speckles move in-plane [1, 9, 6]. These methods are limited due to significant speckle decorrelation when out of plane motion is involved. With the recent development of 3D echocardiography, there has been some effort to track speckles in 3D [3, 12]. However, 3D speckle tracking is a difficult problem since the spatial and temporal resolutions, as well as signal noise ratio, are lower for 3D echocardiography compared to 2D. Thus the speckles are less well defined, exhibit more variability across volumes and more difficult to track.

One important aspect to improve the performance of 3D speckle tracking is the incorporation of spatial and temporal constraints that regularizes the speckle motion, instead of tracking each speckle independently and rely purely on speckle intensities. Motion patterns of adjacent speckles on the myocardium have innate coherence due to their physical proximity, and the heart cycle follows a distinct pseudo-periodic dynamics. Taking advantage of such spatial and

temporal priors is crucial for accurate and robust tracking. In this paper we present a method for tracking speckle patterns in 3D echocardiography sequences. Specifically, we introduce Motion Coherence constraints to the velocity field defined by the speckle motion. This, in conjunction with a dynamics model, can greatly improve the accuracy of 3D speckle tracking.

2. Tracking with Motion Coherence

There has been a long history of regularizing nonrigid motion tracking. Typically elastic splines are used, which uses either the bending energy (second order smoothness constraints) [2, 4] or stretching energy (first order smoothness constraint) or a combination of these two. Regularizing using bending energy leads to thin-plate spline solutions [2]. It is known that in 3D the thin-plate spline solution is not differentiable at point locations. In four or higher dimensions the generalization collapses completely [13].

It is shown that regularizers containing only the first and the second order smoothness constraints are not the most accurate for modeling human cardiac motion [14]. In [14], an extended spline family, called Laplacian spline is used. This spline family minimizes a smoothness constraint functional composed of multiple-order derivative. These different order of derivatives are weighted by some tunable parameters, controlling the amount of corresponding order of smoothness. In [15], it is suggested to penalize an infinite sum of squared all order derivatives of the velocity field to enforce the coherent motion. The idea is that objects close to each other tend to move coherently. In [11], the motion coherence constraint is used for non-rigid point set registration. The regularization term, however, penalizes high frequency content of the velocity field to enforce smooth motion. It shows that the optimal velocity function lies in a span of certain kernel functions defined by the low pass filter. It also shows that when the low pass filter is Gaussian, the regularization term in [11] becomes equivalent to that in [15]. In this paper, we follow the framework of [11] to enforce motion coherence and define efficient algorithm for speckle tracking.

3. Method

3.1. Motion-Coherent speckle tracking

Consider a 3D ultrasound image I_t at time t . We define a speckle as a cubic patch centered at \mathbf{x}_n with intensity vector $\mathbf{a}_n = I_t(\mathbf{x}_n) = [a_n^1, \dots, a_n^K]^T$, where a_n^k is the intensity of the k^{th} voxel in the patch; and K is the total number of voxels in the patch. Assume the speckle patch moves to a new position \mathbf{y}_n in image I_{t+1} , with intensity vector being $\mathbf{b}_n = I_{t+1}(\mathbf{y}_n) = [b_n^1, \dots, b_n^K]^T$. The velocity of the speckle motion is $v(\mathbf{x}_n) = \mathbf{v}_n = \mathbf{y}_n - \mathbf{x}_n$.

Similarly, we define a group of N speckles present in the image I_t at time t as $\mathbf{A}_{N \times K} = [\mathbf{a}_1, \dots, \mathbf{a}_N]^T$ (with coordinates of speckle patch centers at $\mathbf{X}_{N \times 3} = [\mathbf{x}_1, \dots, \mathbf{x}_N]^T$) and at time $t + 1$ in the image I_{t+1} as $\mathbf{B}_{N \times K} = [\mathbf{b}_1, \dots, \mathbf{b}_N]^T$ (with coordinates of speckle patch centers at $\mathbf{Y}_{N \times 3} = [\mathbf{y}_1, \dots, \mathbf{y}_N]^T$). The collective velocity vector of all speckles in the group is $\mathbf{V}_{N \times 3} = [\mathbf{v}_1, \dots, \mathbf{v}_N]^T$. Clearly, $\mathbf{Y} = \mathbf{X} + \mathbf{V}$.

Adopting a Bayesian formulation, we pose the problem of speckle motion estimation between two images I_t and I_{t+1} as finding the velocity vector \mathbf{V} that maximizes the posterior probability $p(\mathbf{V}|\mathbf{B}, \mathbf{A})$. From Bayes rule, we have

$$p(\mathbf{V}|\mathbf{B}, \mathbf{A}) = \frac{p(\mathbf{B}|\mathbf{A}, \mathbf{V})p(\mathbf{V}|\mathbf{A})}{p(\mathbf{B}|\mathbf{A})} \propto p(\mathbf{B}|\mathbf{A}, \mathbf{V})p(\mathbf{V}|\mathbf{A}) \quad (1)$$

The maximum a posteriori (MAP) problem boils down to modeling the likelihood $p(\mathbf{B}|\mathbf{A}, \mathbf{V})$ and the prior $p(\mathbf{V}|\mathbf{A})$. We, now, specify these two terms and motivate our choice. We find it easier to start from the prior, which reflects our belief on the speckle motion.

3.2. Coherence constraint on speckle motion

Physical properties of a cardiac tissue constrain speckles motion to be coherent. For instance, two speckles located close to each other perform similar motion. We formulate such constraint as a smoothness regularization of the velocity field v , defined by the speckles motion. One way of controlling smoothness is by regularizing the high frequency content of the velocity field [11]. Thus, we define the prior on velocity of the speckles motion as

$$p(\mathbf{V}|\mathbf{A}) = \exp^{-\lambda \int_{\mathbb{R}^3} \frac{|\tilde{v}(\mathbf{s})|^2}{\tilde{G}(\mathbf{s})} d\mathbf{s}} \quad (2)$$

where \tilde{v} indicates the Fourier transform of the velocity, λ is a regularization weight and \tilde{G} is real symmetric positive function that approaches zero as $\|\mathbf{s}\| \rightarrow \infty$. In fact, \tilde{G} represents a symmetric low-pass filter, so that its Fourier transform G is real and symmetric [7]. In [11], it is shown that for some choice of the likelihood function, the optimal velocity field function v lies in the span of functions defined by the kernel G . It also shows that when the kernel is chosen to be Gaussian, the prior term in Eq.2 is equivalent to the motion coherence theory introduced in [15], which suggests penalizing a weighted version of all orders of derivative of the velocity field v . Following [11], the optimal velocity field v is of the form

$$v(\mathbf{z}) = \sum_{n=1}^N \mathbf{w}_n G(\mathbf{z} - \mathbf{x}_n) \quad (3)$$

This leads to reparametrization of the velocity vectors using the Gaussian radial basis function: $\mathbf{V} = \mathbf{G}\mathbf{W}$. The

matrix $\mathbf{G}_{N \times N}$ is a square symmetric matrix with elements $g_{ij} = e^{-\frac{1}{2} \left\| \frac{\mathbf{x}_i - \mathbf{x}_j}{\sigma} \right\|^2}$. The Gaussian bandwidth parameter σ controls the locality of the motion coherence constraint. Smaller σ implies only points close to one another should move coherently.

Assuming conditional independence of intensities of the speckle patches given their locations and using Eq. 3, the MAP problem in Eq. 1 is equivalent to minimizing the energy function (for details see [11]):

$$E(\mathbf{W}) = - \sum_{n=1}^N \ln p(\mathbf{b}_n | \mathbf{a}_n, \mathbf{v}_n) + \lambda \text{tr}(\mathbf{W}^T \mathbf{G} \mathbf{W}) \quad (4)$$

where $\mathbf{b}_n = I_{t+1}(\mathbf{y}_n) = I_{t+1}(\mathbf{x}_n + \mathbf{G}(n, \cdot) \mathbf{W})$, $\mathbf{W}_{N \times 3} = (\mathbf{w}_1, \dots, \mathbf{w}_N)^T$ is a matrix of the Gaussian kernel weights in Eq. 3, and $\mathbf{G}(n, \cdot)$ denotes the n^{th} row of \mathbf{G} . Now, we define the likelihood function based on our noise model assumption.

3.3. Noise model

A common noise model is additive Gaussian noise, in which case the likelihood term is equivalent to sum of squared distance. Such a noise model is inaccurate for ultrasound images, where the speckle noise is believed to obey Rayleigh distribution [8, 5]. We adopt the model used in [5], where multiplicative Rayleigh noise model is assumed. The noise model states:

$$b_n^k = s_n^k \cdot n_n^{k(1)}; \quad a_n^k = s_n^k \cdot n_n^{k(2)} \quad (5)$$

where elements s_n^k denotes noiseless value of k^{th} voxel intensity in n^{th} speckle patch, and $n_n^{k(1)}$ and $n_n^{k(2)}$ are two independent noise elements with the Rayleigh density function:

$$p(n) = \frac{\pi n}{2} \exp \frac{-\pi n^2}{4}, \quad n > 0 \quad (6)$$

It follows that

$$b_n^k = a_n^k \cdot \eta_n^k, \quad \text{where } \eta_n^k = \frac{n_n^{k(1)}}{n_n^{k(2)}} \quad (7)$$

The noise term η_n^k is a division of two Rayleigh distributed random variables. Taking the natural logarithm out of both sides of Eq. 7, we obtain logarithm scaled noise model [5], which gives rise to the conditional probability

$$p(b_n^k | a_n^k, \mathbf{v}_n) = \prod_{k=1}^K \frac{2(b_n^k/a_n^k)^2}{((b_n^k/a_n^k)^2 + 1)^2} \quad (8)$$

Substituting Eq. 8 back to the energy function in Eq.4, we obtain the energy function

$$E(\mathbf{W}) = \sum_{n=1}^N \sum_{k=1}^K (-2 \ln b_n^k + 2 \ln[(a_n^k)^2 + (b_n^k)^2]) + \lambda \text{tr}(\mathbf{W}^T \mathbf{G} \mathbf{W}) \quad (9)$$

Motion-Coherent Speckle Tracking

- Given speckle center positions in I_t : \mathbf{X}
- Initialize parameters λ, σ and α
- Construct affinity matrix \mathbf{G} , initiate $\mathbf{W} = 0, \mathbf{Y} = \mathbf{X}$
- Iterate until convergence
 - Construct $\mathbf{a}_n = I_t(\mathbf{x}_n), \mathbf{b}_n = I_{t+1}(\mathbf{y}_n)$
 - Compute \mathbf{P} matrix (Eq. 11)
 - Find $\mathbf{W} = \mathbf{W} - \alpha \mathbf{G}(\lambda \mathbf{W} + \mathbf{P})$
 - Update $\mathbf{Y} = \mathbf{X} + \mathbf{G} \mathbf{W}$
- Final speckle center positions in I_{t+1} : \mathbf{Y}

Figure 1. Pseudo-code of 3D speckle tracking between two volumes: from I_t to I_{t+1} .

3D Speckle Tracking in Full Sequence

- Given speckle centers in the first volume I_1 : \mathbf{X}
- Initialize state $\mathbf{s}_1 = [\mathbf{X}; 0]$
- For $t = 2 : T$ (through all volumes):
 - extract current positions of speckles \mathbf{X} from the state vector \mathbf{s}_{t-1}
 - find new speckle positions \mathbf{Y} in I_t using the motion-coherent tracking algorithm (Fig. 1), given the speckle positions \mathbf{X} in I_{t-1}
 - use \mathbf{Y} as the observation $\mathbf{z}_t = \mathbf{Y}$
 - update the state \mathbf{s}_t using the Kalman filter.

Figure 2. Pseudo-code of 3D speckle tracking through the full sequence of volumes.

3.4. Optimization

By taking the derivative of the energy function E in Eq.9 with respect to \mathbf{W} and equating it to zero, we obtain

$$\frac{\partial E(\mathbf{W})}{\partial \mathbf{W}} = \sum_{n=1}^N \sum_{k=1}^K \frac{\nabla_a b_n^k}{b_n^k} \cdot \frac{(b_n^k)^2 - (a_n^k)^2}{(a_n^k)^2 + (b_n^k)^2} \mathbf{G}^T(n, \cdot) + \lambda \mathbf{G} \mathbf{W} = \mathbf{G} \mathbf{P} + \lambda \mathbf{G} \mathbf{W} = 0 \quad (10)$$

where matrix $\mathbf{P}_{N \times 3}$ is defined with elements

$$p_{nd} = \sum_{k=1}^K \frac{\nabla_a b_n^k}{b_n^k} \cdot \frac{(b_n^k)^2 - (a_n^k)^2}{(a_n^k)^2 + (b_n^k)^2} \quad (11)$$

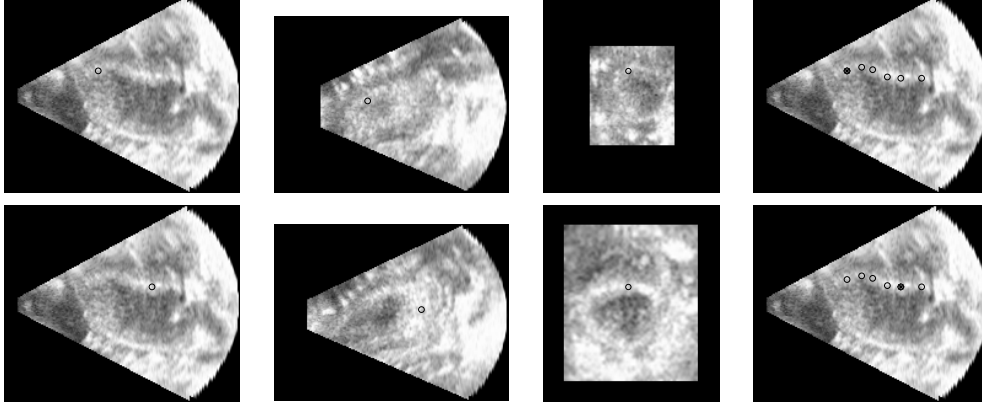


Figure 3. Illustration of two tracked speckles. The first three column shows the 2D slices of the 3D image taken at point coordinate, parallel to the axes. The last column shows all points projected on one plane and with the point of interest emphasized in solid black circle.

Here $\nabla_d b_n^k$ denotes the gradient along direction d of the k^{th} voxel in the n^{th} speckle patch. The explicit solution for \mathbf{W} can not be found, because \mathbf{P} depends on \mathbf{W} . However any gradient based optimization method can be used to find \mathbf{W} iteratively. We use gradient descent algorithm with the update rule being:

$$\mathbf{W} = \mathbf{W} - \alpha \mathbf{G}(\lambda \mathbf{W} + \mathbf{P}) \quad (12)$$

where α is the step size. Given the minimizing \mathbf{W} , the current position of speckle centers in I_{t+1} can be found as $\mathbf{Y} = \mathbf{X} + \mathbf{G}\mathbf{W}$. We summarize the algorithm for finding the speckle positions in image I_{t+1} given speckle positions in I_t in Fig. 1.

3.5. Dynamic models for speckle tracking.

Tracking with motion coherence provides a way of enforcing spatial smoothness for the speckle motion. Speckle motion is also subject to temporal constraint, characterized by the dynamics of the heart motion. We assume a simple process model given by

$$\mathbf{s}_t = \mathbf{F}\mathbf{s}_{t-1} + \mathbf{n}_{t-1}. \quad (13)$$

the state at time $t - 1$ is defined as speckles center positions and their velocities for image I_{t-1} : $\mathbf{s}_{t-1} = [\mathbf{x}_1; \dots; \mathbf{x}_N; \mathbf{v}_1; \dots; \mathbf{v}_N] = [\mathbf{X}; \mathbf{V}]$. Matrix \mathbf{F} is defined as

$$\mathbf{F}_{6N \times 6N} = \begin{pmatrix} \mathbf{I}_{3N \times 3N} & \mathbf{I}_{3N \times 3N} \\ \mathbf{0}_{3N \times 3N} & \mathbf{I}_{3N \times 3N} \end{pmatrix}$$

Process noise \mathbf{n}_{t-1} is assumed to have Gaussian distribution $p(\mathbf{n}) \sim \mathcal{N}(\mathbf{0}, \mathbf{R})$. We define the measurement model by

$$\mathbf{z}_t = \mathbf{H}\mathbf{s}_t + \mu_t \quad (14)$$

Here the measurement (observation) is defined as locations of the speckle centers. Matrix $\mathbf{H}_{3N \times 6N}$ is given by

$[\mathbf{I}_{3N \times 3N}; \mathbf{0}_{3N \times 3N}]$. The measurement noise μ_t is assumed to have Gaussian distribution with $p(\mu) \sim \mathcal{N}(\mathbf{0}, \mathbf{Q})$.

The discrete Kalman filter can be used to update the above system. The measurement at time t that is used to update the predicted state. The measurement is obtained by tracking the speckle locations from time $t - 1$ using motion-coherent tracking summarized in Fig. 1. We summarize the 3D speckle tracking algorithm for the full sequence in Fig. 2.

4. Results

We show the performance of 3D speckle tracking on a set of 3D echocardiography sequences from open chest porcine hearts. One of the hearts has severe ischemia. The scans are acquired using Philips Sono 7500 with EKG gating. We use detected post-scan converted images with echo envelop signals, represented in the Cartesian coordinates. The spatial resolution is $160 \times 144 \times 192$ voxels. Ten different scans (3D sequences) are taken. Each scan consists of ten 3D volumes. We run the experiments for each of the scans individually. For each scan, in the first volume, we manually initiate a set of points (varying from 5-9) on the myocardium, and run our speckle tracking method.

The algorithm is implemented in Matlab, and tested on a Pentium4 CPU 3GHz with 4GB RAM. The value of smoothness parameters are set to $\lambda = 1$, $\sigma = 15$. The size of the speckle patch is $17 \times 17 \times 17$. For the Kalman filter, process and measurement noise covariance are set to $\mathbf{Q} = 0.2 * \mathbf{I}$, $\mathbf{R} = 0.01 * \mathbf{I}$. The stopping condition for the motion-coherent iterative process is either when the current change in energy function drops below the threshold of $1e-5$ or the number of iterations reaches the maximum of 100. On average the motion-coherent tracking algorithm between two volumes converges in less than one minute and requires around 30 iterations.

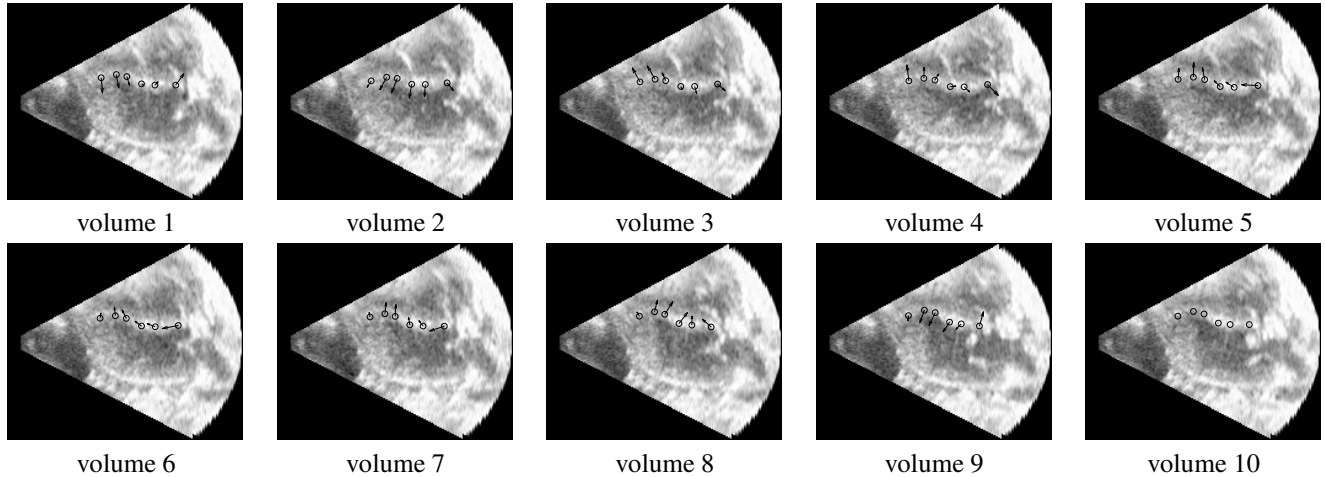


Figure 4. Illustration of tracked speckles and their velocities for a complete scan of 10 volumes, by enforcing motion coherence.

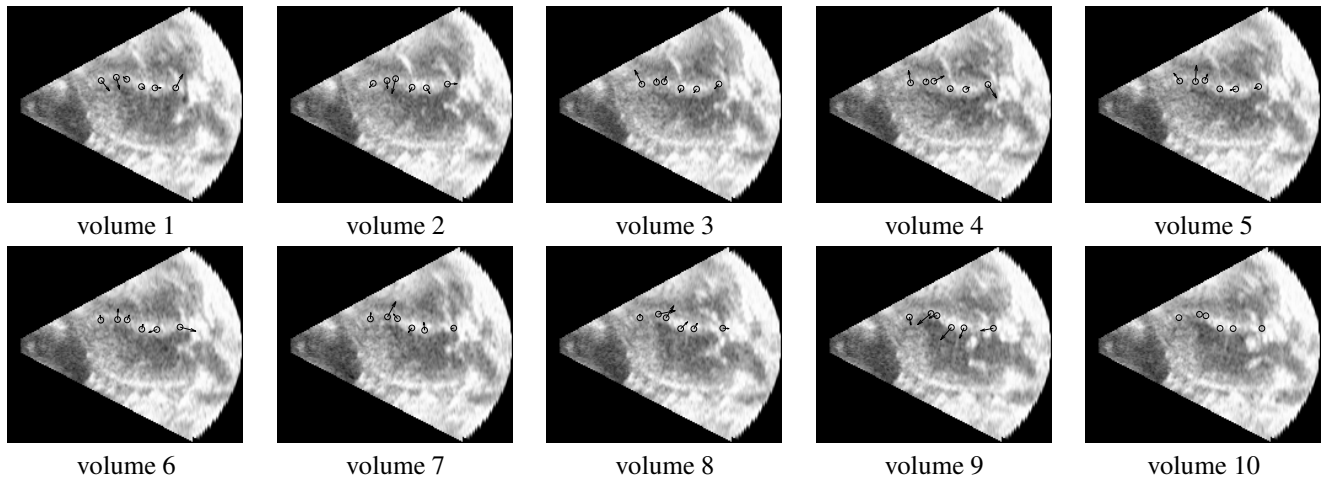


Figure 5. Illustration of tracked speckles and their velocities for a complete scan of 10 volumes, without enforcing motion coherence.

To validate the results, we obtain the ground truth of the speckle locations by manually tracking them across the whole sequence. A cardiologist is asked to track the speckles manually, given its initial locations, using a tool to visualize and select the points from arbitrary 2D cross sections of 3D volume. We compare our automated speckle tracking using the described algorithm against the ground truth. The tracking error for a speckle patch at a given volume in a given scan is defined by the 3D Euclidean distance between the tracked position and ground truth. The tracking error (averaged over all scans, volumes and number of speckles) is 0.3224 ± 0.1597 voxel.

Figure 3 illustrates the tracked locations of two example speckles in a scan with a total of six speckles. The first row shows speckle 1, and the second row shows speckle 5. First three columns show the 3D location of each speckle in a given volume projected onto three 2D planes, represented

by black circles. The last column show how speckles 1 and 5 relate to the rest of tracked speckles, all projected onto the same 2D plane. As we can see the two example speckles lie nicely on the heart wall as expected.

Figure 4 illustrates the tracking results of the full sequence of 10 volumes, showing the 3D velocity of all tracked points projected onto a 2D plane for easy visualization. The velocity vectors exhibit local smoothness, as a result of enforcing motion coherence. To demonstrate the effect of coherence constraint, we also track the speckles without any regularization (Fig. 5). In this case the velocities of the speckle patches are tracked independently from one another. We can clearly see that without motion coherence constraint, the velocity vectors exhibit randomness in both direction and amplitude, even for neighboring speckles, which is inaccurate. In fact, the average tracking error is 2.4508 ± 2.2100 voxel without motion coherence constraint,

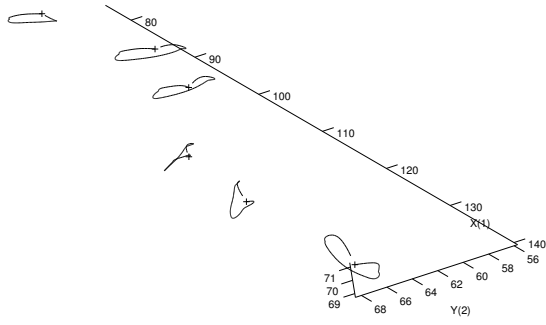


Figure 6. Illustration of tracked 3D trajectories of six speckles for a complete scan of 10 volumes. Symbol "+" denotes starting location of the speckle.

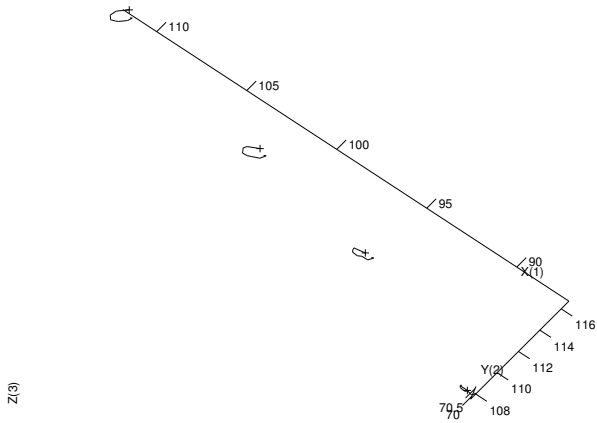


Figure 7. Illustration of 3D trajectories of speckles from an ischemic heart region. The motion is limited.

much worse than that with the constraint.

In Fig. 6, we illustrate the 3D trajectories of tracked speckles. The speckles demonstrate significant through-plane motion, justifying for the need of tracking in 3D. Speckle positions can be effectively used for strain estimation. Strain is a geometrical expression of deformation, expressed as a relative change in length. Given the speckle locations, the strain is measured by calculating the change in distance between speckles in time, *i.e.*, $\varepsilon = \frac{l-l_0}{l_0} = \frac{\Delta l}{l_0}$, where l_0 and l are the initial and current distance between speckle centers in 3D. Figure 8 and 9 illustrate the distance and the strain between two speckles.

The algorithm can effectively identify the ischemic region of the heart. Figure 7 shows the trajectories of speckles that are placed on the ischemic region. Figure 10 shows their velocities through the whole sequence. It is clear that the motion is very limited for the ischemic heart tissue, compared to the normal tissue (Fig. 6 and Fig. 4). In fact, the average length of speckles motion for the whole se-

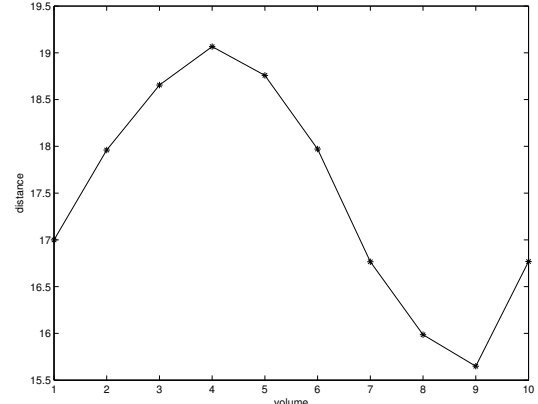


Figure 8. Distance between 5th and 6th tracked speckles.

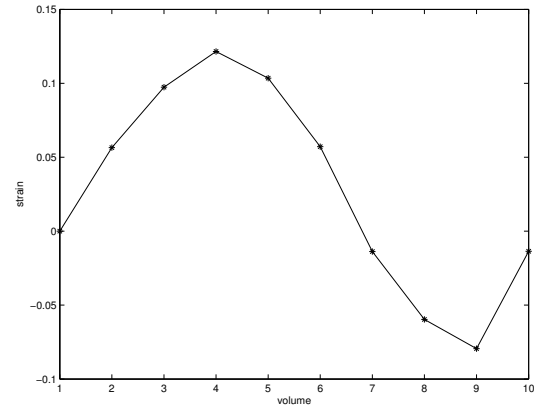


Figure 9. Strain between 5th and 6th tracked speckles.

quence from the ischemic region is 3.2370 ± 0.9323 voxel. In contrast, that of the normal tissue from the same heart is 14.3106 ± 2.4085 voxel.

5. Discussions and conclusions

We present a method for 3D ultrasound speckle tracking and describe a framework to enforce motion coherence. The motion coherence constraint helps the nearby speckles to move coherently. For instance, if one of the speckles tends to move incorrectly, as part of the group, it has to obey the motion pattern of the other speckles. To force the coherent motion, we regularize the velocity field to be smooth; we follow the coherence regularization proposed for non-rigid point set registration [11] and show how speckle tracking benefits from such regularization. We also take advantage of the dynamic model to assure the temporal smoothness of the speckle trajectory.

We use a similarity function based on a multiplicative Rayleigh noise model assumption, which is proved to work better than sum-of-squared-differences and normal-

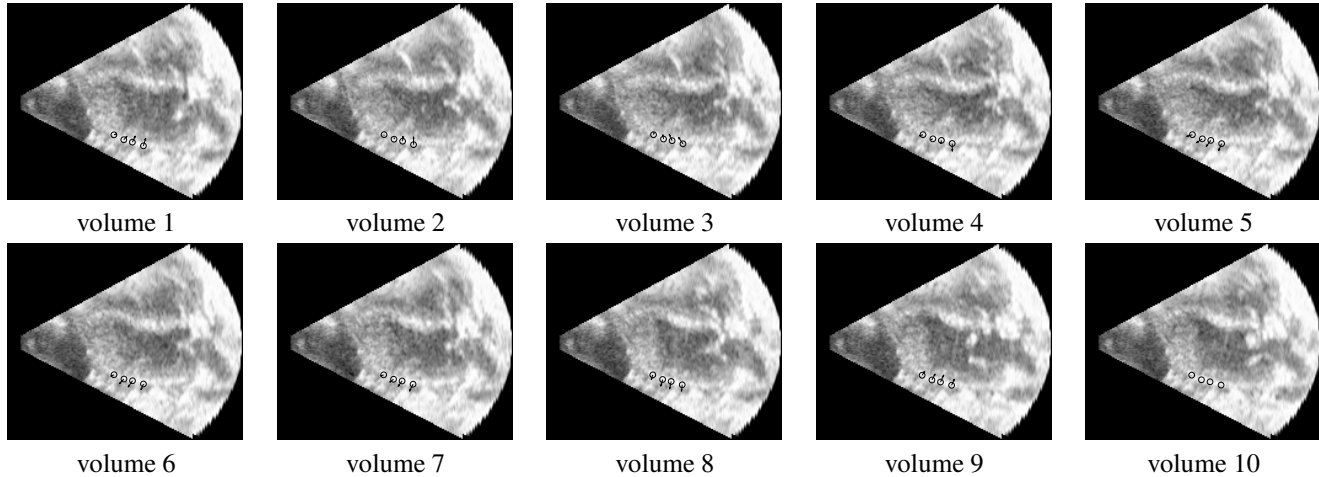


Figure 10. Illustration of speckle motions from an ischemic heart region.

ized cross-correlation for the ultrasound data [5].

We use 3D ultrasound post-scan converted envelop images; the RF data may provide extra information in the axial direction, however, the computational efforts increase significantly due to the large amount of the data to process. We demonstrate the performance of the method on 10 different 3D echocardiography scans from open chest porcine hearts. The method shows accurate and robust performance.

Future directions include the adoption of more accurate and sophisticated heart dynamics for speckle tracking and the integration of speckle tracking with boundary motion to better characterize heart deformation.

References

- [1] L. Bohs, B. Geiman, M. Anderson, S. Gebhart, and G. Trahey. Speckle tracking for multi-dimensional flow estimation. *Ultrasonics*, 38:369–375, 2000.
- [2] F. L. Bookstein. Principal warps: Thin-plate splines and the decomposition of deformations. *PAMI*, 11(6):567–585, June 1989.
- [3] X. Chen, H. Xie, R. Erkamp, K. Kim, C. Jia, J. Rubin, and M. O’Donnell. 3-D correlation-based speckle tracking. *Ultrasonic Imaging*, 27:21–36, 2005.
- [4] H. Chui and A. Rangarajan. A new algorithm for non-rigid point matching. *CVPR*, 2:44–51, 2000.
- [5] B. Cohen and I. Dinstein. New maximum likelihood motion estimation schemes for noisy ultrasound images. *Pattern Recognition*, 35:455–463, February 2002.
- [6] J. d’Hooge, B. Bijmens, J. Thoen, F. van de Werf, G. Sutherland, and P. Suetens. Echocardiographic strain and strain-rate imaging: a new tool to study regional myocardial function. *IEEE Transactions on Medical Imaging*, 21(9):1022–1030, Sept. 2002.
- [7] F. Giroi, M. Jones, and T. Poggio. Priors stabilizers and basis functions: From regularization to radial, tensor and additive splines. 1993.
- [8] C. Kontogeorgakis, M. Srintzis, N. Maglaveras, and I. Kokkinidis. Tumor detection in ultrasound b-mode images through motion estimation using a texture detection algorithm. 1994.
- [9] M. Ledesma-Carbayo, J. Kybic, M. Desco, A. Santos, and M. Unser. Cardiac motion analysis from ultrasound sequences using non-rigid registration. In W. Niessen and M. Viergever, editors, *Proc. of Medical Image Computing and Computer Aided Intervention*, pages 889–896, 2001.
- [10] T. Makela, P. Clarysse, O. Sipila, N. Pauna, Q. C. Pham, T. Katila, and I. Magnin. A review of cardiac image registration methods. *IEEE Transactions on Medical Imaging*, 21(9):1011–1021, 2002.
- [11] A. Myronenko, X. Song, and M. Carreira-Perpinan. Non-rigid point set registration: Coherent point drift. In B. Schölkopf, J. Platt, and T. Hoffman, editors, *Advances in Neural Information Processing Systems 19*. MIT Press, Cambridge, MA, 2007.
- [12] I. Pratikakis, C. Barillot, and P. Helier. Robust multi-scale non-rigid registration of 3d ultrasound images. In M. Kerchhove, editor, *Scale-Space 2001*, pages 389–397, 2001.
- [13] R. Sibson and G. Stone. Computation of thin-plate splines. *SIAM J. Sci. Stat. Comput.*, 12(6):1304–1313, 1991.
- [14] D. Suter and F. Chen. Left ventricular motion reconstruction based on elastic vector splines. *IEEE Transactions on Medical Imaging*, 19(4):295–305, 2000.
- [15] A. Yuille and N. Grzywacz. The motion coherence theory. *International Journal of Computer Vision* 3, pages 344–353, 1988.